

# Electrocatalytic Palladium Nanoclusters as Versatile Indicators of Bioassays: Rapid Electroanalytical Detection of SARS-CoV-2 by Reverse Transcription Loop-Mediated Isothermal Amplification

Alejandro Rodríguez-Penedo, Pablo Rioboó-Legaspi, Andrea González-López, Ana Lores-Padín, Rosario Pereiro, María del Mar García-Suárez, María Dolores Cima-Cabal, Estefanía Costa-Rama, Beatriz Fernández,\* and M. Teresa Fernández-Abedul\*

Quantitative polymerase chain reaction (qPCR) is considered the gold standard for pathogen detection. However, improvement is still required, especially regarding the possibilities of decentralization. Apart from other reasons, infectious diseases demand on-site analysis to avoid pathogen spreading and increase treatment efficacy. In this paper, the detection of SARS-CoV-2 is carried out by reverse transcription loop-mediated isothermal amplification, which has the advantage of requiring simple equipment, easily adaptable to decentralized analysis. It is proposed, for the first time, the use of palladium nanoclusters (PdNCs) as indicators of the amplification reaction at end point. The pH of the medium decreases during the reaction and, in turn, a variation in the catalytic activity of PdNCs on the oxygen reduction reaction (ORR) can be electrochemically observed. For the detection, flexible and small-size screen-printed electrodes can be premodified with PdNCs, which together with the use of a simple and small electrochemical equipment would greatly facilitates their integration in field-deployable devices. This would allow a faster detection of SARS-CoV-2 as well as of other future microbial threats after an easy adaptation.

## 1. Introduction

In recent years, there has been an enormous interest in developing analytical devices that enable rapid and decentralized medical diagnostics, especially at the point-of-care (POC).<sup>[1]</sup> This supposes a turning point for patients and consumers, as well as for healthcare professionals, leading to a real transformation of current healthcare systems.


The pandemic caused by SARS-CoV-2 has accentuated the need to develop quick and robust analytical methodologies, producing highly precise and accurate results.<sup>[2]</sup> Although research has been intense, it must continue to be ready to fight against future microbiological threats. Easy-to-use lateral flow immunoassays, with low price and small size are appropriate for on-site diagnostics,<sup>[3]</sup> but still offer low sensitivity,<sup>[4,5]</sup> reporting a significant percentage of false positives cases.<sup>[4]</sup>

In contrast, assays based on quantitative PCR (qPCR), considered the most effective by the World Health Organization,<sup>[6]</sup> has the advantage of high reliability. Although some adaptation to POC devices is found in the bibliography,<sup>[7]</sup> the integration of optical detection, that requires relatively complex equipment,<sup>[8]</sup> and the use of ramps of temperature, make it difficult. Thus, the use of isothermal strategies such as loop-mediated isothermal amplification (LAMP, or RT-LAMP if reverse transcription is required) is introduced as an alternative to temperature cycling. This facilitates decentralized testing allowing faster (< 1 h), cheaper,<sup>[9]</sup> and easier to perform procedures,<sup>[10]</sup> while maintaining similar detection limits as well as sensitivity and selectivity.<sup>[11]</sup>

Apart from gel electrophoresis, turbidimetric and colorimetric detection<sup>[12]</sup> are the most used methods for LAMP detection. Colorimetric approaches take advantage of the fact that during the amplification procedure pyrophosphate ions and protons are released. Thus, the indicator hydroxynaphthol blue allows monitoring the change in concentration of  $Mg^{2+}$ , ions that

A. Rodríguez-Penedo, P. Rioboó-Legaspi, A. González-López, A. Lores-Padín, R. Pereiro, E. Costa-Rama, B. Fernández, M. T. Fernández-Abedul  
Department of Physical and Analytical Chemistry  
University of Oviedo  
Oviedo 33006, Spain  
E-mail: fernandezbeatriz@uniovi.es; mtfernandeza@uniovi.es

M. del M. García-Suárez, M. D. Cima-Cabal  
School of Engineering and Technology  
International University of La Rioja  
Logroño 26006, Spain

 The ORCID identification number(s) for the author(s) of this article can be found under <https://doi.org/10.1002/adhm.202202972>

© 2023 The Authors. Advanced Healthcare Materials published by Wiley-VCH GmbH. This is an open access article under the terms of the Creative Commons Attribution-NonCommercial License, which permits use, distribution and reproduction in any medium, provided the original work is properly cited and is not used for commercial purposes.

DOI: 10.1002/adhm.202202972

precipitate with phosphate.<sup>[13]</sup> Similarly, the use of pH-sensitive dyes produces a color change.<sup>[14]</sup> Also noteworthy is the rise of platforms based on microfluidics as lateral flow analysis on paper. An application is the early diagnosis of hepatitis C using the RT-LAMP technique with detection based on lateral flow nucleic acid strips.<sup>[15]</sup> Combining RT-LAMP and lateral flow assays with vertical flow sample processing has allowed decentralized malaria diagnosis in rural communities.<sup>[16]</sup> Similarly, the use of paper-origami DNA microfluidics has been applied to the diagnosis of bovine infectious reproductive diseases.<sup>[17]</sup> In all the cases, detection by the naked eye either from visible spots or their fluorescence emission using a hand-held torch or digitally with a mobile-phone camera, have been employed.

Electrochemical detection (ED) has also been employed<sup>[18,19]</sup> being very appropriate to the development of POC devices, due to its low cost, ease to use, portability and high sensitivity.<sup>[20]</sup> For example, the use of methylene blue, which can act as a redox intercalating probe, is the basis of an electrochemical sensor that allows the detection of SARS-CoV-2 in wastewater.<sup>[21]</sup> Regarding the change in pH, electrochemistry has traditionally been the preferred technique for measuring this parameter. Therefore, direct measurement has been demonstrated using a solid-state hydrogen ion selective electrode sensor fabricated on graphene-modified screen-printed electrodes.<sup>[22]</sup> Similar electrodes (screen-printed electrodes previously coated with reduced graphene) have been modified with pH-sensitive conducting polyaniline to measure the change in the open circuit potential for end-point detection of LAMP reactions.<sup>[23]</sup>

Metal nanoclusters (MNCs) consist of a spherical cluster of atoms, ranging from a few tens to several hundreds, whose size is close to the Fermi wavelength.<sup>[24]</sup> This causes the energy bands typical of metal nanoparticles (NPs) to be split into discrete energy levels, so that the MNCs exhibit optoelectronic and chemical properties different from NPs and metal complexes. They can be synthesized using protective ligands that interact with the metal, creating a layer that improves their stability, while allowing the MNCs to solubilize in aqueous media when using ligands with a hydrophilic terminal end.<sup>[25,26]</sup> Small thiolated organic molecules are appropriate ligands because the thiol groups interact strongly with the metal, producing very stable bonds.<sup>[26]</sup> Regarding the metal, gold,<sup>[27]</sup> and silver<sup>[28]</sup> NCs are the most common, although other metals such as platinum<sup>[29]</sup> or palladium<sup>[30]</sup> are also of high interest. MNCs have been successfully employed in a wide range of fields, such as bioimaging,<sup>[31]</sup> cell labeling,<sup>[32]</sup> theranostics,<sup>[33]</sup> and catalysis.<sup>[29,34]</sup>

PdNCs have been found to possess catalytic activity on several electrochemical reactions,<sup>[34,35]</sup> such as the hydrogen evolution reaction (HER)<sup>[36,37]</sup> or the oxygen reduction reaction (ORR),<sup>[38–40]</sup> that happens at lower negative potential. The general ORR mechanism depends directly on the pH of the electrolyte (acidic or alkaline). In any case, multiple electron transfer occurs, with final conversion to H<sub>2</sub>O or OH<sup>−</sup>, respectively.<sup>[41]</sup> In either electrolyte, two possible pathways can be adopted, a direct 4 e<sup>−</sup> reduction or an indirect route with two consecutive 2 e<sup>−</sup> reductions. In the last case, the first step generates H<sub>2</sub>O<sub>2</sub> or HO<sub>2</sub><sup>−</sup> as intermediate species, in acidic or basic electrolytes, respectively, that are further reduced to H<sub>2</sub>O or OH<sup>−</sup>. Dissociative (for the direct way) and associative (for direct/indirect ways) mechanisms are possible. In basic medium, after adsorption of O<sub>2</sub> in the cat-

alytic active site (O<sub>2</sub><sup>\*</sup>), the dissociative route involves cleavage of the bond O–O to form 2 adsorbed O<sup>\*</sup> species that are reduced gaining two protons and two electrons to form 2 OH<sup>\*</sup>. Finally, they form 2 OH<sup>−</sup> by gaining two electrons. However, in the associative 4 e<sup>−</sup> way, O<sub>2</sub><sup>\*</sup> is reduced in a one proton/one electron transfer process to form OOH<sup>\*</sup>, that is further reduced producing O<sup>\*</sup> and OH<sup>−</sup> (1 e<sup>−</sup> transfer process). The reduction of O<sup>\*</sup> to OH<sup>\*</sup> involves again one proton/one electron transfer. Finally, in the fourth 1 e<sup>−</sup> transfer step, OH<sup>\*</sup> forms OH<sup>−</sup>, that is desorbed regenerating the catalytic active site (\*). In the associative indirect (two 2 e<sup>−</sup> transfer steps) route, the OOH<sup>\*</sup> produced by O<sub>2</sub><sup>\*</sup> reduction, is reduced again and desorbed to form OOH<sup>−</sup>. The reduction is completed with the generation of OH<sup>−</sup>, with a final balance of 4 OH<sup>−</sup> produced with participation of 1 O<sub>2</sub> and 2 H<sub>2</sub>O molecules. In the case of acidic electrolytes, the 4 H<sup>+</sup> required are transferred directly from the medium. Following dissociative or associative mechanisms depends on the O<sub>2</sub> dissociating energy barrier on a surface. A parallel mechanism, combination of both dissociative and associative routes is also possible.<sup>[42]</sup>

Regarding the material, Pd has demonstrated to be an excellent catalyst, being better substrate to support Pt catalyst monolayers when compared with Au, Pt, and Ir, showing Pt<sub>monolayer</sub>/Pd (111) the highest activity among the surfaces studied, even higher than pure Pt(111)<sup>[43]</sup> and with the smaller difference between activation energy barriers of bond-breaking and bond-making steps.<sup>[42]</sup> In this context, plots of oxygen reduction activity against O and OH binding energies shows that Pt and Pd are the best catalysts for oxygen reduction.<sup>[44]</sup> The suitability of Pd as electrocatalyst is also demonstrated by the increase in the ORR rate of Pd-modified Au clusters, compared with bare Au clusters,<sup>[45]</sup> opening the door to engineering ultrasmall noble metal clusters with high area-volume ratios and robust stabilities for ORR.<sup>[41]</sup> Although in most of the cases acidic or basic electrolytes have been employed, important catalytic activity over ORR has been demonstrated also in neutral media, by modification of glassy carbon electrodes (GCEs) with colloidal dispersions of Pd nanostructures.<sup>[46]</sup> In this context, Au-Pd nanoparticles performed even better than Pt nanoparticles in the neutral media, required for microbial fuel cells.<sup>[47]</sup>

Several authors have exploited the different catalytic properties of PdNCs for multiple applications. Generation of PdNCs by electrodeposition from a PdCl<sub>2</sub> solution was employed for developing, e.g., a sensor for catecholamine neurotransmitters and paracetamol,<sup>[48]</sup> or a nonenzymatic sensor for hydrogen peroxide.<sup>[49]</sup> PtPdNPs were also synthesized and used as modifiers, together with acetylcholinesterase, of a GCE for organophosphate pesticide detection.<sup>[50]</sup> In all these cases, electroactive species were measured on the modified electrodic surface. However, analytical applications based on the catalytic activity of PdNCs on ORR are very scarce. Hybrid Pd-AuNCs have been used as tags for the detection of hyaluronidase wound infection biomarker in a magnetic bead-based immunoassay.<sup>[51]</sup>

However, to the best of our knowledge, the catalytic activity of PdNCs has never been used as the basis of the detection of a LAMP amplification of genetic material. MNPs have been used in the detection of genetic material after RT-LAMP amplification,<sup>[52]</sup> but their catalytic effect has not been the basis of the detection. Thus, human papillomavirus 16 E6/E7 mRNA has been detected using AuNPs as support of thiolated DNA strands that hybridize

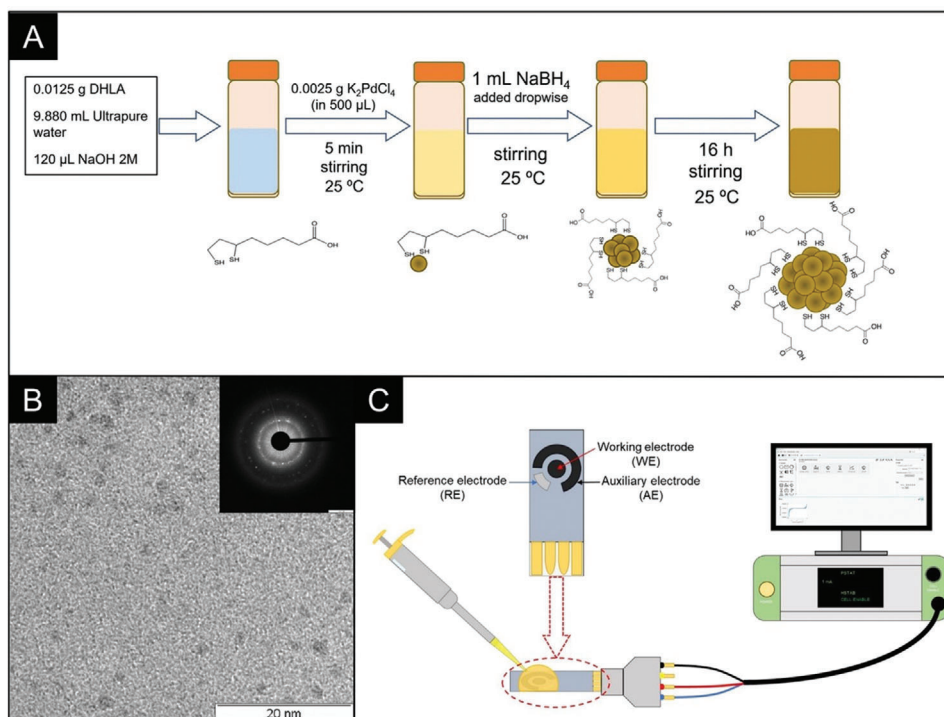


**Figure 1.** A) Schematics of the PdNCs synthesis procedure. B) HR-TEM image obtained for the PdNCs with the SAED image in the inset. C) Schematics of the electrochemical measurement setup.

with biotinylated amplicons. After incubation and centrifugation, AuNPs were deposited on a GCE for further enzymatic detection with streptavidin conjugated HRP and TMB. This is the first time, to the best of our knowledge, that PdNCs (or other NCs) are used for the detection of amplification of genetic material.

The kinetics of oxygen reduction at Pd electrodes varies with the pH of the medium.<sup>[53]</sup> Thus, we hypothesize that, as the catalytic effect of PdNCs on ORR could also vary with the pH, which changes during a LAMP reaction, the variation of an electrical magnitude (e.g., potential or intensity of current) related to the PdNCs catalytic activity, could be the analytical signal that correlates with the number of initial copies of genetic material.

Thus, in this work, PdNCs with catalytic activity on ORR will be synthesized in neutral medium and characterized by microscopy and electrochemical techniques. In an innovative strategy, these PdNCs will be used for the first time as indicators of LAMP reactions. In this way, SARS-CoV-2 detection can be based on the change in the catalytic effect of the PdNCs due to the variation of pH produced during the amplification, allowing them to differentiate between positive and negative samples.

## 2. Results and Discussion

### 2.1. Synthesis and Characterization of PdNCs

A procedure to allow the synthesis of stable PdNCs with catalytic activity was carried out. Thus,  $K_2PdCl_4$  was used as a precursor salt,  $NaBH_4$  as a reducing agent and DL-6,8-thioctic acid (DHLA) as a thiolated protective agent. DHLA is a bidentate ligand that provides great stability to the PdNCs due to the chelate effect.<sup>[26]</sup>

The procedure for the synthesis of PdNCs is detailed in the Experimental Section, and schematically represented in **Figure 1A**. After addition of all the reagents, growing of PdNCs took place for 16 h under stirring. According to image of the PdNCs obtained by HR-TEM (Figure 1B), the metallic core of the PdNCs was  $1.69 \pm 0.06$  nm on average (99% confidence interval with  $n = 148$ , using the standard normal distribution). Since NCs diameter can be close to SEM resolution limit and higher resolution images can be obtained by HR-TEM, this technique was preferred over SEM. The selected area electron diffraction (SAED) technique was also used to obtain the structure of the crystal of PdNCs, which was found to be FCC (face centered cubic). By knowing both the average diameter of the PdNCs and the crystal lattice structure, the number of Pd atoms per NC can be obtained. It was found to be 172 atoms of Pd per NC on average.

The synthesized PdNCs have been characterized by absorbance spectroscopy (Figure S1, Supporting Information) as well as by inductively coupled plasma-mass spectrometry (ICP-MS), whereby the concentration of Pd in the purified solution of PdNCs was found to be  $40.2 \pm 1.1 \mu\text{g mL}^{-1}$ . PdNCs were also characterized using energy-dispersive X-ray spectroscopy (Figure S2, Supporting Information) to ensure that the images obtained by HR-TEM correspond to PdNCs.

### 2.2. Evaluation of PdNCs Electrocatalytic Properties

Cyclic voltammetry (CV) was employed to examine the electrochemical processes in which PdNCs are involved. For such purpose, the electrochemical behavior of PdNCs in three different

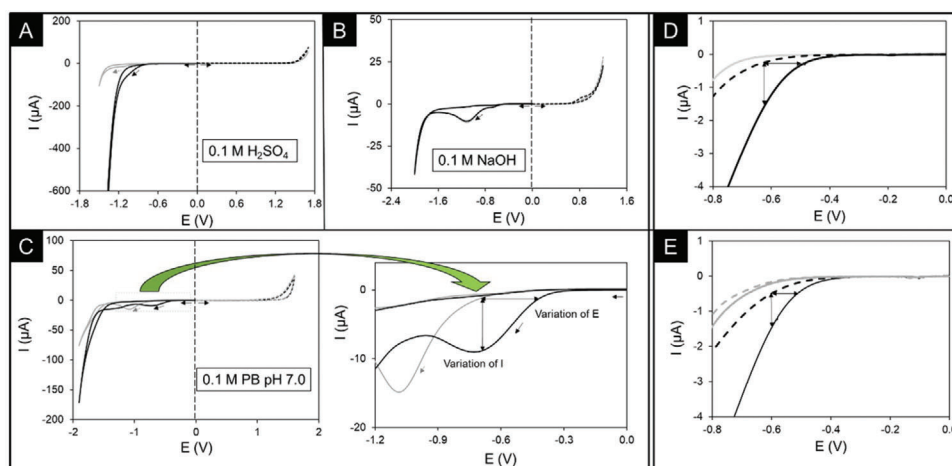


**Figure 2.** CVs recorded in different solutions, without (gray line) and with  $1.6 \mu\text{g mL}^{-1}$  of PdNCs (black line): A)  $0.1 \text{ M H}_2\text{SO}_4$ , B)  $0.1 \text{ M NaOH}$ , and C)  $0.1 \text{ M PB pH } 7.0$ , scanned toward negative (solid line) and positive (dashed line) potentials. In C), a zoom of the area marked is presented at the right. D) Effect of the rate of  $\text{NaBH}_4$  addition: LSVs recorded in  $0.1 \text{ M PB pH } 7.0$ , with  $1.6 \mu\text{g mL}^{-1}$  of PdNCs synthesized by quick (all at once; continuous black line) or slow addition (1 drop every 5 s; dashed black line). E) Effect of deoxygenation: LSVs recorded in  $0.1 \text{ M PB pH } 7.0$  solutions, with  $1.6 \mu\text{g mL}^{-1}$  of PdNCs before (continuous black line) and after bubbling  $\text{N}_2$  for 5 min (dashed black line). In gray, LSVs of solutions without PdNCs.

media ( $0.1 \text{ M H}_2\text{SO}_4$ ,  $0.1 \text{ M NaOH}$ , and  $0.1 \text{ M}$  phosphate buffer (PB)  $\text{pH } 7.0$ ) was studied. In all the cases, a concentration of  $1.6 \mu\text{g mL}^{-1}$  of PdNCs was used, obtained by dilution of the stock solution ( $40.2 \mu\text{g mL}^{-1}$ ) in the corresponding media. **Figure 2A,B,C** shows the voltammograms obtained in each of the tested media with (black line) and without (gray line) PdNCs. In each case, two scans were recorded: one toward negative potentials (solid line) and the other in the positive direction (dashed line). Scans were started at  $0.0 \text{ V}$  in both cases, where no electrolysis was observed.

In **Figure 2A**, which shows the CVs recorded in acid medium, it can be observed how the reduction process, namely HER (hydrogen evolution reaction), is catalyzed by the PdNCs. A movement toward less negative potentials, which corresponds to an increase of  $111 \mu\text{A}$  (in absolute value) at a potential of  $-1.2 \text{ V}$ , is noticed. No other remarkable reduction or oxidation processes related to the catalytic activity of the PdNCs were observed. On the other hand, in voltammograms recorded in basic medium ( $0.1 \text{ M NaOH}$ ), HER and ORR, as well as oxygen evolution reaction (OER) processes, can be clearly observed. However, it seems that PdNCs do not exhibit any remarkable catalytic effect on these reactions. A small anodic process at about  $+0.8 \text{ V}$ , close to the background electrolyte oxidation, is also observed, which has been attributed to the oxidation of the DHLA coating the PdNCs.<sup>[53]</sup> In **Figure 2C**, the voltammograms recorded in neutral medium ( $0.1 \text{ M}$  phosphate buffer,  $\text{pH } 7.0$ ) are shown. Here, it can be seen some catalytic activity on HER, although much less remarkable than the obtained in acidic medium. Likewise, PdNCs also seem to have catalytic activity on ORR. For better visualization of the difference between the voltammograms recorded in the buffer solution with and without PdNCs, a zoomed graph is shown in **Figure 2C**.

Therefore, PdNCs possess catalytic activity both on ORR (and slightly on HER) when working in neutral medium and on HER when working in acid medium. Here we focused on the PdNCs catalytic activity on ORR (in neutral medium), since the applica-

tion to pathogen detection by LAMP is performed at pH values comprised between  $\approx 6$  and  $8$ . Considering that only a cathodic process is involved, in further studies only linear sweep voltammograms (LSVs) toward negative potential values were recorded instead of the whole cyclic voltammogram.

In the zoom of **Figure 2C**, the two possibilities for quantifying the catalytic effect are shown, either measuring the variation of the potential at a given intensity of current or, the variation of the current intensity at a given potential. Both will be assessed in the optimization of the PdNCs synthesis to obtain stable PdNCs with the highest catalytic activity on ORR, to ascertain which is one is the best analytical signal.

The catalytic activity of metal nanoclusters has been found to depend on multiple factors, such as size,<sup>[54]</sup> shape,<sup>[55]</sup> and the amount of ligand with which they are coated.<sup>[39]</sup> To obtain MNCs with the desired catalytic properties, it is necessary to optimize the synthesis conditions. It has been usually found that increasing the temperature at which the synthesis is performed leads to an increase in the size of the PdNCs.<sup>[56]</sup> Also, the addition of the reducing agent is the key step to control the formation of MNCs.<sup>[57]</sup> Thus, it was decided to optimize both the rate of addition of  $\text{NaBH}_4$  and the temperature at which the synthesis is carried out to obtain PdNCs with the highest catalytic activity on ORR. **Figure S3A, S3B** shows the absorbance spectra obtained by adding  $\text{NaBH}_4$  quickly and slowly, and for the different temperatures tested, respectively.

**Figure 2D** shows the difference in the voltammograms recorded in solutions of PdNCs synthesized adding the reducing agent quickly (directly with the micropipette) or slowly, at a rate of 1 drop every 5 s. As can be seen in **Figure 2D**, the PdNCs synthesized adding quickly the reducing agent show remarkable catalytic activity at about  $-0.60 \text{ V}$ , while those synthesized by adding the reducing agent slowly show a signal much less distinguishable from the background. Additionally, the effect of the temperature at which the synthesis was performed has also been evaluated and is shown in **Figure S4** (Supporting Information). It can

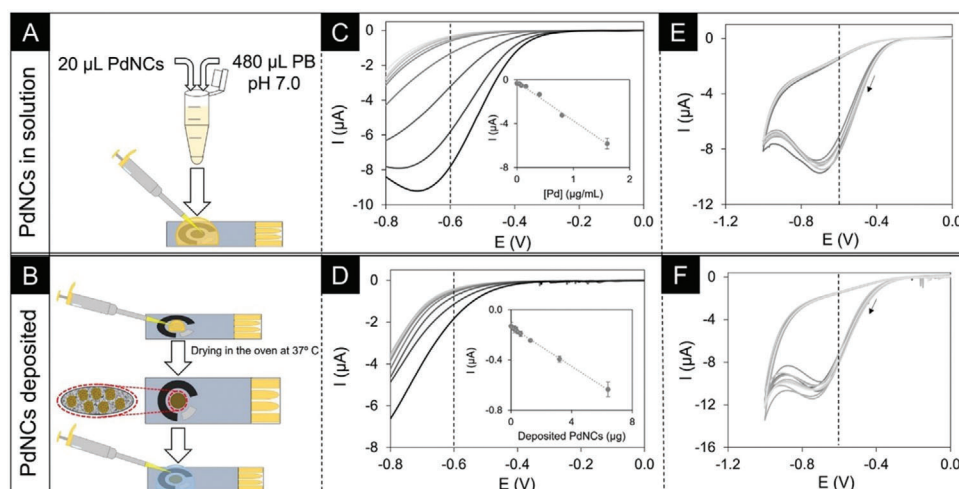


**Figure 3.** Schematic of the measurement protocol with: A) PdNCs in solution and, B) deposited on the WE. LSVs obtained for different concentrations of PdNCs: C) in solution and, D) deposited on the electrode, showing the calibration plots obtained in both cases as an inset (error bars represent the standard deviation of the mean for 3 replicates ( $n = 8$ )). Ten CVs recorded successively for: E)  $1.6 \mu\text{g mL}^{-1}$  of PdNCs in solution and, F)  $64 \mu\text{g}$  of PdNCs deposited on the WE.

be here observed that PdNCs synthesized at constant temperature of  $15^\circ\text{C}$  have lower catalytic activity on ORR than those obtained at higher temperature of  $25^\circ\text{C}$  (current intensity of  $-5.9 \pm 0.2 \mu\text{A}$  vs  $-7.1 \pm 0.3 \mu\text{A}$  at a potential of  $-0.60 \text{ V}$ ). Likewise, no significant differences were found between those synthesized at  $25$  and  $40^\circ\text{C}$ . Then, the lower temperature was chosen according also to energy saving. Only the synthesis with the highest catalytic activity ( $25^\circ\text{C}$ , quick addition of  $\text{NaBH}_4$ ) was characterized by HR-TEM, EDX, and SAED.

To demonstrate that the electrochemical process observed at  $\approx -0.60 \text{ V}$  in  $0.1 \text{ M}$  PB solutions corresponds to ORR, LSVs were recorded in a PdNCs solution (1:25 dilution of the stock in buffer) with and without removing the oxygen. Then, voltammograms were recorded in drops of a PdNCs solution before and after bubbling  $\text{N}_2$  for 5 min. The results obtained (Figure 2E) show that the electrochemical process is significantly reduced after  $\text{N}_2$  bubbling, which clearly indicates that it corresponds to ORR. The slight difference with the signal recorded in the buffer, suggests that either  $\text{O}_2$  has not been completely removed from the solution, or that new molecules are rapidly dissolved in the short time preceding the measurement.

### 2.3. Analytical Characteristics of PdNCs-Based Voltametric Methodology

The catalytic activity of PdNCs on ORR at neutral medium have been used to determine the PdNCs concentration and the analytical characteristics of the methodology were assessed. Reusability of electrodes was first evaluated. For this purpose, 10 consecutive measurements were recorded using a single electrode, washing it thoroughly in between, first with ultrapure water and then with the buffer solution (Figure S5A, Supporting Information). Measurements were recorded in  $1.6 \mu\text{g mL}^{-1}$  PdNCs solutions in  $0.1 \text{ M}$  PB pH 7.0. The results show that the first measurement is the one with the highest signal, gradually decreasing in the fol-

lowing ones. Consequently, a new SPCE was used for each measurement.

So far, experiments have been recorded in solutions containing PdNCs, but they could be also previously deposited on the working electrode (WE) surface. In this case, CVs were recorded after adding the selected buffer. Both methodologies are explained in the diagrams shown in Figure 3A,B, for the PdNCs in solution and the deposited PdNCs, respectively. Procedures are detailed in the Experimental Section.

Thus, the reusability of the electrodes with immobilized PdNCs was evaluated by depositing  $6.4 \mu\text{g}$  on the working electrode and recording 5 CVs, washing the electrode in between. Figure S5B (Supporting Information) shows the results obtained, being similar to those obtained in the case of PdNCs added in solution, with a less pronounced decrease.

Then, the variation of the electrochemical signal with PdNCs concentration (either in solution or deposited on the electrode) was studied. LSVs recorded for concentrations ranging from  $0.1$  to  $4.0 \mu\text{g mL}^{-1}$  are shown in Figure 3C. A linear relationship between the intensity of the current recorded at  $-0.60 \text{ V}$  and the concentration of PdNCs was obtained ( $R^2 = 0.994$ ,  $n = 8$ ), with a sensitivity of  $-3.5 \mu\text{A mL}^{-1}$ . The limit of detection (LOD), calculated as the concentration corresponding to 3 times the standard deviation of the intercept, was found to be  $0.04 \mu\text{g mL}^{-1}$ .

The same experiment was performed depositing the PdNCs directly on the electrode. Figure 3D shows the voltammograms obtained for different  $\mu\text{g}$  of PdNCs deposited on the electrode (between  $0.21$  and  $6.4 \mu\text{g}$ , following the procedure described in the Experimental Section). An amount of  $6.4 \mu\text{g}$  of PdNCs deposited on the electrode dissolved in  $40 \mu\text{L}$  of buffer are equivalent to  $0.16 \mu\text{g mL}^{-1}$  of PdNCs in solution. The intensity of the current measured at  $-0.60 \text{ V}$  varied linearly ( $R^2 = 0.998$ ,  $n = 8$ ) with the concentration of PdNCs deposited, with a sensitivity of  $-7.8 \mu\text{A mL}^{-1}$ . The LOD was  $0.12 \mu\text{g}$  of deposited PdNCs, which is equivalent to  $3.1 \text{ ng mL}^{-1}$  of PdNCs if they would have been dissolved in the buffer solution. In this way, comparing both LODs,

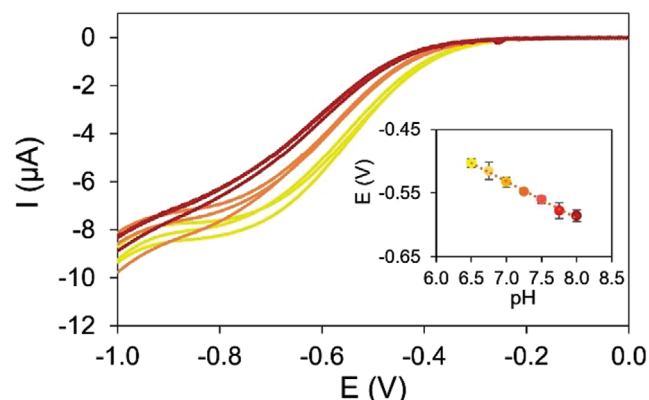


**Figure 4.** LSVs recorded with PdNCs-modified electrodes (320 µg of Pd deposited) on 40 µL 10 mM Tris-HCl pH 6.50 (yellow), 7.25 (orange), and 8.00 (red). Three voltammograms are recorded for each pH. In the inset, the potential at which a current of  $-3 \mu\text{A}$  is reached is represented versus pH. The error bars correspond to the standard deviation of the mean for three replicates ( $n = 7$ ).

lower concentrations of PdNCs could be detected if they were deposited directly on the electrode.

The reproducibility of the measurements (using one electrode for each measurement) was evaluated from 10 voltammograms recorded in drops of a solution with a concentration of  $1.6 \mu\text{g mL}^{-1}$  of PdNCs (Figure 3E) and in buffer solution on electrodes with 64 µg of deposited PdNCs (Figure 3F). The intensity of the current measured at a potential of  $-0.60 \text{ V}$  was found to be  $-7.8 \pm 0.4$  and  $-7.8 \pm 0.3 \mu\text{A}$  for PdNCs in solution or deposited, respectively. The value obtained for the relative standard deviation (RSD) was 5.0% and 4.7%, respectively, indicating an adequate precision of the methodology.

## 2.4. Effect of pH in Catalytic Activity of PdNCs

It has been previously reported that the catalytic activity of Pd over ORR (using Pd electrodes) is affected by the pH of the solution.<sup>[58]</sup> To evaluate this effect using PdNCs deposited on carbon electrodes (320 µg of Pd, i.e., 8 µL of the undiluted PdNCs solution) LSVs were recorded on 40 µL of 10 mM Tris-HCl buffer of the corresponding pH. It has been observed the variation of the potential varied for a current of  $-3 \mu\text{A}$ .

Figure 4 shows the voltammograms recorded for pH 6.50, 7.25, and 8.00 (three in each case). It was found a linear variation between potential and pH in a range comprised between 6.50 and 8.00, as shown in the inset of Figure 4. The relationship fitted to a straight line ( $R^2 = 0.995$ ,  $n = 7$ ), being the slope  $-0.0574 \text{ V per pH unit}$ . This relationship could be the basis of analytical methodologies where a pH change is implied. This is the case of LAMP reactions, that use slightly buffered media.

## 2.5. Electrochemical Detection of SARS-CoV-2

The variation of the catalytic activity of PdNCs on ORR with their concentration allows them to be used as labels of bioreagents to determine species bioanalytically. In addition, those species that

produce a pH change in the medium can be monitored by following the pH change. This is the case of LAMP amplifications of nucleic acids.

The concentration of PdNCs should be kept constant and a variation either in the potential or intensity of current of ORR can be directly attributed to the extension of the reaction and thus to the initial number of copies of genetic material. Since this is an isothermal amplification and electrochemical techniques are intrinsically simple, this methodology is of enormous interest for the decentralized detection of pathogens causing infectious diseases, such as the case of SARS-CoV-2. As a proof of applicability, PdNCs are used as indicators for detection of SARS-CoV-2 using LAMP reaction, the rationale for which is shown in Figure S6 (Supporting Information). Since this coronavirus is RNA-based, a previous step of reverse transcription (RT) must be added (RT-LAMP). The N1 fragment of SARS-CoV-2,<sup>[59]</sup> has been selected for amplification using the primers described in the Experimental Section, selected based on a published work.<sup>[60]</sup>

The medium used to carry out the isothermal amplification contains phenol red, a pH indicator that allows visual differentiation between negative (red) and positive (orange/yellow) LAMP reactions. Phenol red is also electroactive, so it is also possible to differentiate them by electrochemical techniques.<sup>[61,62]</sup> Apart from the detection by the naked eye, the measurement of the variation with pH of the catalytic activity of PdNCs over ORR is more precise and sensitive alternative, never used before for detecting amplifications of genetic material. Exploring this approach is justified by the urgency of being ready to face appropriately future biothreats.

To check that the pH of the medium did indeed decrease as amplification proceeded, it was decided to perform amplifications by quadruplicate at different levels of concentration, i.e., 107, 330, and 1070 initial copies/µL. The pH, measured with a microelectrode capable of measuring in very small sample volumes ( $<24 \mu\text{L}$ ), was  $7.5 \pm 0.12$ ,  $6.9 \pm 0.16$ , and  $6.63 \pm 0.06$ , respectively. The value for the negative control, also measured, was  $7.8 \pm 0.25$  (discarding one tube). It presented a notable difference with the lowest concentration level considered. The variation found in pH makes possible to use PdNCs as electrochemical indicators, as will be discussed later.

A calibration curve for different number of initial copies of the N1 sequence of SARS-CoV-2, comprised between 107 and 2148 copies  $\mu\text{L}^{-1}$  of standard solution is presented in Figure 5A, with pictures of the end-point amplifications performed in septuplicate, except for 1432 and 2148 number of copies  $\mu\text{L}^{-1}$ , which were performed in quadruplicate due to RNA availability, in microcentrifuge tubes. As the RT-LAMP kit employed contains phenol red as visual pH indicator, a difference in color between negative (red) and positive (orange or yellow) reactions can be observed. This is more clearly evidenced at  $4 \text{ }^\circ\text{C}$ . Six out of seven negative controls show an intense red color. A variation to different tones of orange and yellow is observed for amplifications with increasing number of copies  $\mu\text{L}^{-1}$ . A table summarizing semiquantitative results after naked-eye color observation is shown in the “visual detection” section of Figure 5B.

Apart from this detection, other optical methods that measure color differences, such as those based on smartphone-assisted image processing software (e.g., using ImageJ) and absorbance measurements were evaluated for further comparison with the

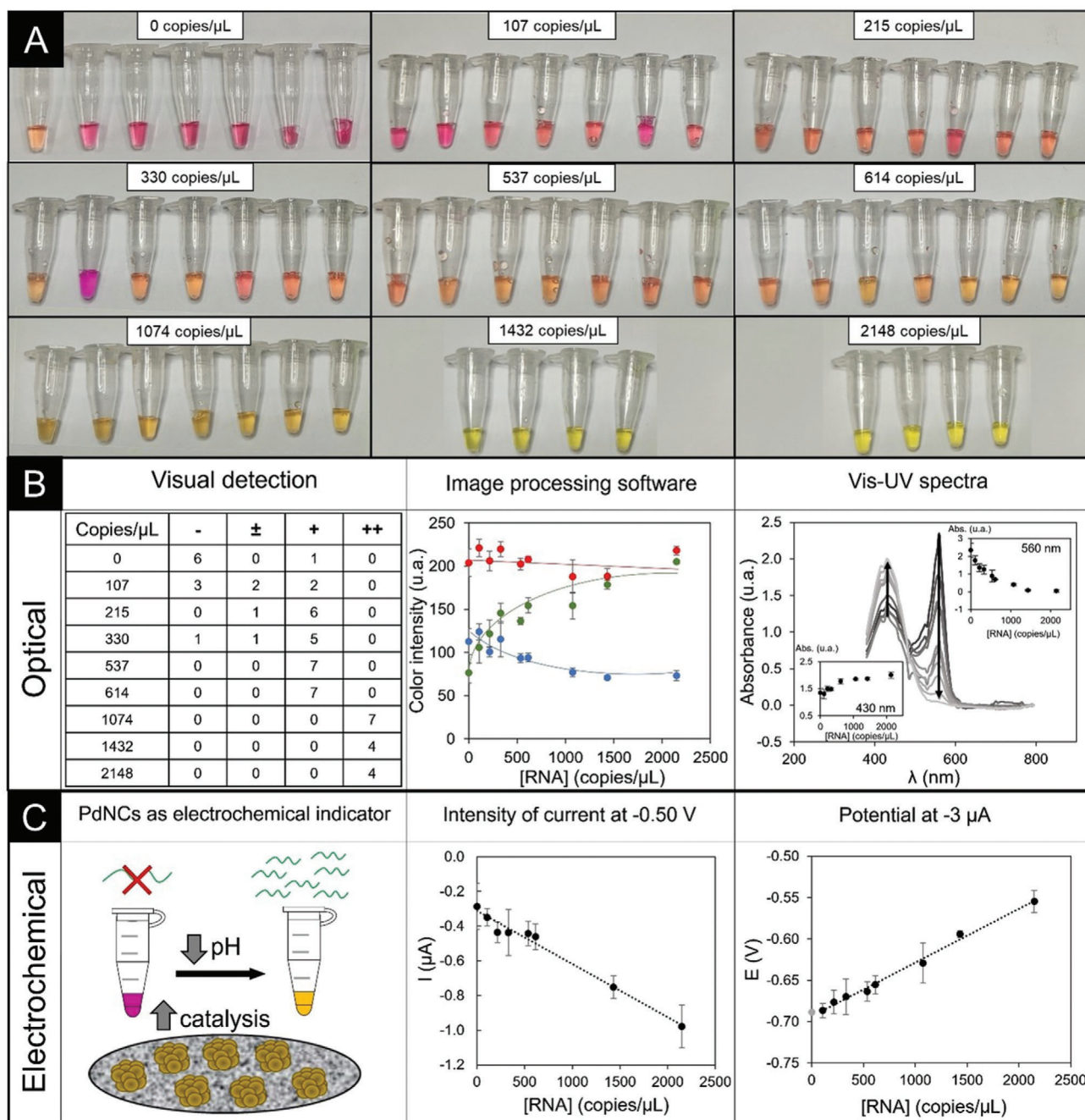


**Figure 5.** Amplifications performed using SARS-CoV-2 RNA copies comprised between 107 and 2148 initial copies of the N1 fragment/μL. A) Photograph showing the color of the solutions after amplification. B) Optical detection: (left) visual detection, with “-” for samples classified as negative (red), “±” for doubtful samples and “+” (orange) or “++” (yellow) for the positive ones, (center) results of image processing software and (right) visible absorption spectra. Error bars show the standard deviation of the mean of 7 measurements. C) Electrochemical detection: (left) schematics of the procedure based on the catalytic activity of PdNCs, and calibration curves based on the measurement of the intensity of the current ( $n = 8$ ) (center), and the potential ( $n = 8$ ) (right). Error bars show the standard deviation of the mean of 9 (from 107 to 1074 copies  $\mu\text{L}^{-1}$ ) or 6 (for 1432 and 2148 copies  $\mu\text{L}^{-1}$ ) measurements.

electrochemical methodology based on the use of PdNCs. For image processing (Figure 5B), the image captured by the camera of a smartphone was divided into the three RGB channels, with no significant variation in the red channel. The differences found when processing both blue and green channel images were much more noticeable. The results obtained when comparing the color

intensity in the blue channel showed a clear trend toward a decrease in color for amplifications with higher RNA concentration. On the contrary, when using the color intensity in the green channel, it seemed to increase as the initial RNA concentration increased. On the other hand, Figure 5B shows the visible-UV spectra recorded with equipment that allows measurements in

volumes less than 24  $\mu\text{L}$ . Two peaks can be seen for all the tubes. The peak at 430 nm (associated with deep blue color) increased with the number of initial copies meanwhile the peak at 560 nm (associated with green/yellow) showed the opposite effect, being more intense for the negative control.

Electrochemical approaches using PdNCs as indicators are reported in Figure 5C. The first part of the figure shows schematically the basis of the methodology used to employ PdNCs as electrochemical indicators. The results obtained, either when measuring the potential at  $-3 \mu\text{A}$  or the intensity of the current produced at  $-0.50 \text{ V}$  are shown at the right. The measurements were carried out using membranes on the electrodes (as stated under the Experimental Section) to reduce the volume required for measurement, so that only 10  $\mu\text{L}$  were employed. In this way, two voltammograms were recorded per tube. It can be seen in both cases that the graphical representation of the intensity of current or potential, respectively, versus the initial RNA copy number per  $\mu\text{L}$  fits properly to a straight line. In the first case, a slight linear fit ( $R^2 = 0.98$ ,  $n = 8$ ), with a slope of  $-3 \times 10^{-4} \mu\text{A} (\text{copies}/\mu\text{L})^{-1}$  was found, with values of cathodic current (negative) increasing for increasing RNA concentration. The representation of the potential measured at an intensity of  $-3 \mu\text{A}$  fitted much better ( $R^2 = 0.991$ ,  $n = 8$ ) with a slope of  $7 \times 10^{-2} \text{ mV} (\text{copies}/\mu\text{L})^{-1}$ , with values of the potential (negative) decreasing for increasing RNA concentration. The value for the negative control (whose potential was  $-0.681 \text{ V}$ ) was indicated in gray. Therefore, it was considered that the measurement of the potential at a certain intensity was a more appropriate analytical signal.

End-point detection usually limits the dynamic range, being this very close to the LOD. However, here is where instrumental measurements could help to avoid false results. To evaluate the practical LOD of the developed methodology for RT-LAMP detection, 10 negative and 10 positive amplification reactions (i.e., containing 0 and 100 copies of the fragment N1 of SARS-CoV-2  $\mu\text{L}^{-1}$ ) were performed. Figure S7 (Supporting Information) shows the corresponding box and whiskers plot, using the potential at which an intensity of current of  $-3 \mu\text{A}$  is attained as analytical signal. It can be seen a significant difference between negative and positive amplifications, with average values of  $-0.598$  and  $-0.533 \text{ V}$ , respectively. Atypical values were not detected. The median was slightly closer to the first quartile for negative values and more centered for positive reactions. The interquartile range, which represents the 50% of the results, was as low as 0.015 V for negative values, indicating a very low dispersion. In the case of the 100 copies  $\mu\text{L}^{-1}$  the interquartile range resulted higher: 0.066 V. The maximum value for negative reactions was  $-0.571 \text{ V}$ , meanwhile the minimum for the positive was  $-0.593 \text{ V}$ , indicating a slight overlap of the whiskers. Then, a concentration of initial copies of SARS-CoV-2 of 100 copies  $\mu\text{L}^{-1}$  is considered as the practical LOD of the methodology. In any case, a set of negative reactions must be always carried out because variations between different lots of the RT-LAMP kit, which include biological reagents, or slight differences in the potential measured using screen-printed carbon electrodes (SPCEs) of different batches can occur. On the other hand, LAMP can give false positives due to cross contamination and interactions between (heterodimer) or within (autodimerization) primers (nonspecific amplification). For the first case, we have used uracil-DNA-glycosylase<sup>[63]</sup> which eliminates most of the false positives. For the second case, some

compounds seem to solve the problem,<sup>[64]</sup> but they should be tested in the future to see if they influences the sensitivity of the amplification. The use of higher temperatures (e.g.,  $65 \text{ }^\circ\text{C}$  instead of  $60 \text{ }^\circ\text{C}$ ) and appropriate surface decontamination also reduces this problem.<sup>[65]</sup>

In the **Table 1**, the electrochemical detection approach here proposed is compared, in a qualitative way, with pH measurement and different optical detection strategies. Lateral flow-based systems for further detection of amplicons have also been considered.<sup>[66,67]</sup> These constitute an approach that interfaces amplification with detection, that can be mainly visual, based on image capture and processing or optical instrumental measurements. Thus, they are included in between both, and the qualification will depend on the detection employed.

Regarding to the cost, since visual detection does not require any equipment, and smartphone-assisted image processing could use a smartphone or camera to take high quality images are cheaper than instrumental measurements. Lateral flow platforms, usually with visual readout, can be also considered low-cost devices, although it must be taken into consideration that they require additional reagents for the detection. Both electrochemical methodologies require simple instrumentation (micro pHmeter or potentiostat, respectively), as well as some consumables, which represents a relatively low cost. In terms of analysis time, all of them take just a few minutes to perform the procedure (except for visual detection, which is virtually instantaneous), although absorbance spectroscopy can be considered faster due to the easily automated data postprocessing. Both absorbance spectroscopy and PdNCs-based voltammetry are very simple, requiring only the correct use of a micropipette. If the supplied electrodes were premodified with PdNCs it would be even simpler and cheaper. To find out whether this is possible, a study of the stability of PdNCs-modified electrodes has been carried out. It was observed that the electrocatalytic activity of PdNCs deposited on the electrodes remain stable for one week (stored at room temperature and protected from light), with only a 10% reduction in the current intensity (at  $-0.60 \text{ V}$ ) after 2 weeks (Figure S8, Supporting Information). Lateral flow-based systems are also extremely easy to use, but some expertise is required if quantitative analysis is aimed. Regarding the pH measurement, its complexity lies in the fact that the required microelectrode for measuring low-volume samples is extremely fragile. In the case of image processing, valid photographs, under the same illumination and absence of reflections, as well as a correct processing of images and subsequent data are required.

Instrumental measurements are appropriate for quantitative analysis, being these based on visual detection more adequate for qualitative or semiquantitative analysis. Depending on the detection system, lateral flow-based methodologies allow to perform semiquantitative analysis (turbidimetry),<sup>[67]</sup> or quantitative.<sup>[68]</sup> The use of PdNCs allows the quantification of the initial concentration of RNA copies. Regarding portability, both absorbance spectrophotometry and pH measurement seem rather difficult to adapt to decentralized analysis. However, modified microelectrodes that allow pH measurements, which would be easily decentralized, were reported.<sup>[19]</sup> Visual detection is intrinsically decentralized, as well as lateral flow platforms, although in this case it depends on the detection principle employed. In the case of images captured with a smartphone and subsequent processing,



**Table 1.** Comparison of the characteristics of different detection methods for RT-LAMP: PdNCs-based voltammetric methodology, pH measurement and optical methodologies, including lateral flow-based strategies.

Detection method	Low cost	Fast	Easy to use	Quantitative analysis	Decentralization
Visual detection	+++	+++	+++	+	+++
Smartphone-assisted image processing	+++	++	++	+	+++
Lateral flow-based systems	+++	++	+++	++	+++
Absorbance spectroscopy	+	++	++	++	+
pH measurement	++	++	++	++	++
PdNCs-based voltammetry	++	++	+++	+++	+++

Code: (+++) good, (++) acceptable and (+) poor.

high quality pictures (with homogeneous lighting), and further processing must be considered. Detection using PdNCs as electrochemical indicators with possibility of using miniaturized potentiostats, PdNCs-modified electrodes and simple procedures is very promising, especially when done simultaneously with visual detection, because this instrumental measure is useful in classifying dubious results.

### 2.6. Electrochemical Determination of SARS-CoV-2 in Nasopharyngeal Samples for Human Donors

To prove the applicability of the methodology, four nasopharyngeal exudate samples, collected at the Central University Hospital of Asturias (HUCA), were analyzed for detection of SARS-CoV-2. Specifically, two of the samples were taken from COVID-19 patients (determined by PCR) and two from healthy control subjects. **Figure 6A** shows a photograph of the different amplifications carried out, also including a negative control (aqueous solution). Although the negative control and negative samples cannot be distinguished visually (both the control and samples are of red color) a slight difference can be appreciated electrochemically (**Figure 6B**). An evident change in color is observed for positive samples and, also, significant differences between negative and positive samples are observed when the electrochemical approach based on PdNCs was followed (**Figure 6B**). To study if quantification was possible, positive samples were 1:2 diluted up to  $\approx 600$  copies  $\mu\text{L}^{-1}$ . For these diluted samples, the LAMP reactions provided an orange color (**Figure 6A**). Using the PdNCs as indicators, it is possible to differentiate negative from those diluted positive samples, as can be seen in **Figure 6B**. **Table S2** (Supporting Information) shows the results obtained by PCR and by PdNCs-based ED of RT-LAMP reactions.

In this way, it has been proven by the first time, that voltammetry on PdNCs-modified electrodes can be used for detection of (RT)-LAMP reactions, by measuring the decrease in the potential of the catalysis of PdNCs on ORR. As the measurement is based on an instrumental readout, this methodology possesses special interest in those reactions where visual detection becomes difficult. It also allows the use with other LAMP master mixes, even without including phenol red. This said, a dual detection (visual and instrumental) would be very useful to avoid false results. On the other hand, it must be considered that the LAMP methodology is based on the use of a weakly buffered solution to allow for visual detection. This low buffering capacity required to trigger

the pink to yellow color change limits sample compatibility, as highly buffered sample inputs or acid samples may impact the color change.<sup>[69]</sup> In this work, we have successfully assessed nasopharyngeal exudate with no interferences but, regarding the impact of the sample on the method, each sample, as it presents its own inherent characteristics, would have to be considered separately.

Work is in progress to integrate reaction and detection, taking advantage of the small size of the electrochemical instrumentation required and the isothermal character of the amplification. Decentralization will allow to be ready for fighting against further biothreats,<sup>[70]</sup> with low-cost equipment that can be easily deployed in field. This integration will approach real-time measurements without requiring tube-to-electrode transfer, allowing to access the end user with simpler procedures and lower analysis times.

### 3. Conclusions

A simple electrochemical methodology that employs stable and monodisperse PdNCs (characterized by absorbance spectroscopy, ICP-MS, EDX, and HR-TEM) with catalytic activity on ORR has been employed, for the first time, to detect SARS-CoV-2 by RT-LAMP. The reduction of the pH of the medium as the amplification proceeds also produces a linear variation in the potential at which ORR occurs, which was correlated to the number of initial copies of RNA. Electrodes can be previously modified with PdNCs, which simplified the procedure. SARS-CoV-2 was determined in nasopharyngeal exudate samples from human donors, with significant differences between negative and positive results. This methodology demonstrates the possibilities of metallic nanoclusters, in this case through the detection of RT-LAMP reactions of SARS-CoV-2 genetic material. The main advantages could be summarized as: i) It allows non-subjective quantitative measurements with simple equipment: premodified screen-printed electrodes and potentiostat; ii) A linear response close to the (low) LOD permits decreasing the number of false results; iii) The instrumental readout does not depend on external optical conditions (illumination), end-user (visual) skills, or equipment facilities (smartphone camera, optics); iv) Electrochemical cells are disposable, not requiring cleaning procedures (as happens with, e.g., pH-electrodes for small-volume measurements); v) Indirect measurement through the catalytic activity of PdNCs on the ORR avoids the addition of electrochemical probes

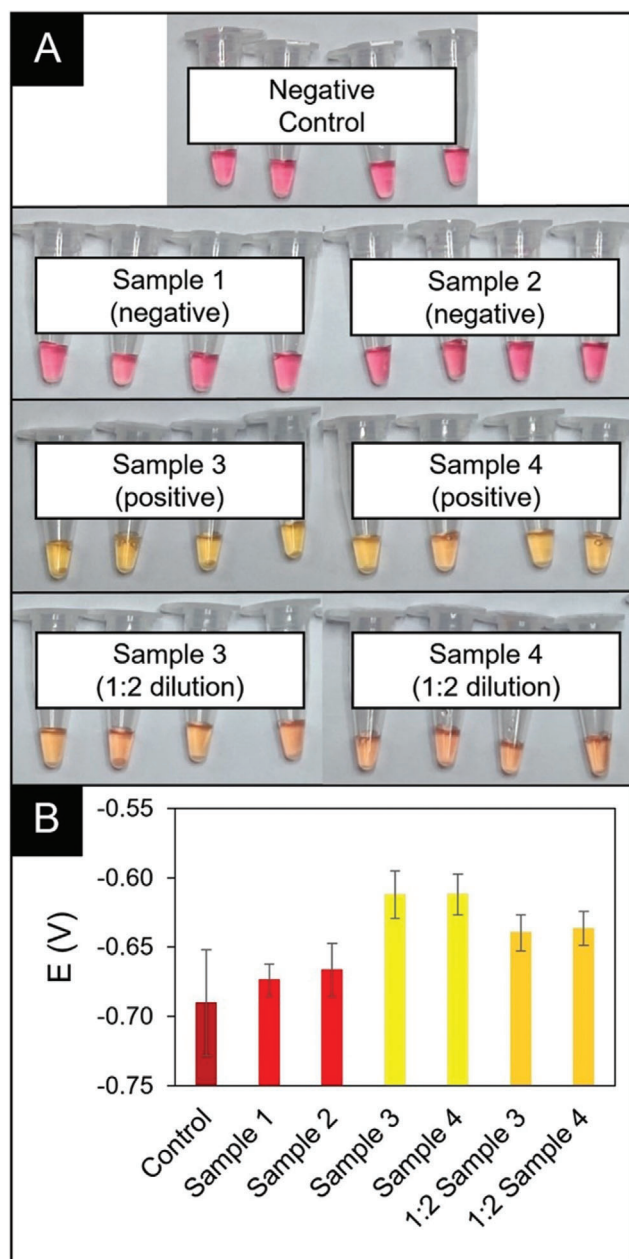


**Figure 6.** Analysis of nasopharyngeal swab samples: A) Picture of LAMP reactions for negative and positive samples (undiluted and 1:2 diluted), as well as a negative control. B) Bar chart showing the analytical signal (potential at which an intensity of current of  $-3 \mu\text{A}$  is reached) obtained for each one of the analyzed samples. Error bars show the standard deviation of the mean of 4 measurements.

to the amplification kit. Thus, the methodology can be combined with LAMP master mixes that do not include indicators; vi) Since the ORR is a reduction process, interferences that could come from the oxidation of interfering species are avoided, and finally; vii) The low cost and portability of the equipment, together with the simplicity of the procedure favor decentralization.

This methodology paves the way to the full integration of LAMP reactions and electrochemical detection (LAMP-ED). This

would allow continuous operation with on-line amplification-detection of this disease and other future pathogenic threats, approaching real-time quantification.

#### 4. Experimental Section

**Materials and Reagents:** For the synthesis of PdNCs, potassium tetrachloropalladate (purity  $\geq 99.99\%$ , Sigma-Aldrich; USA) was used as the salt precursor. DL-6,8-Thioctic acid, reduced (purity  $\geq 98\%$ , Sigma-Aldrich, India) was used as ligand. The reduction of the palladium salt was carried out using sodium borohydride (purity  $> 98\%$ , Sigma-Aldrich, USA). The basic solution required for the synthesis was prepared using sodium hydroxide (purity  $> 98\%$ , Sigma-Aldrich, USA).

Amicon Ultra-0.5 (membrane PLBC, 10 kDa, Millipore Amicon, Ireland) was used for the purification of PdNCs.

Phosphate buffer solution was prepared using disodium hydrogen phosphate anhydrous and sodium dihydrogen phosphate dihydrate (both purity 100%, VWR Chemica, Belgium). A 0.1 M  $\text{H}_2\text{SO}_4$  solution was prepared with sulfuric acid (purity 95–97%, Merck, Germany). A 0.1 M NaOH solution was prepared out using sodium hydroxide (purity  $> 98\%$ , Sigma-Aldrich; USA). Ultrapure water was used, with a resistivity of 18.2 M $\Omega$  cm (Pure-lab Flex 3; ELGA-Veolia, UK).

**Instruments:** The PdNCs synthesis has been performed under constant stirring at 25 °C with the help of a stirrer-heating plate (IKA RCT basic, IKA Werke, Germany). Weighing was carried out using a precision analytical balance (NewClassic MF, Mettler Toledo, Spain).

A minicentrifuge (Gyrozen and Co; Daejeon, South Korea) was used for purification procedures. The pH was measured using a pH-meter (Crison micropH 200, Crison Instruments S.A., Spain) with micro pH electrode (Orion 9863BN Micro pH Electrode, Thermo Fisher Scientific) capable of measuring in 0.5  $\mu\text{L}$ .

Absorbance measurements were performed using a spectrophotometer (Cary 60 UV-VIS, Agilent Technologies; USA) with a Suprasil quartz fluorescence cuvette (model 114F-QS, Sigma-Aldrich), which has an optical path of 10 mm and a chamber volume of 3 mL. To measure the absorbance in the amplifications a PICOPET01 spectrophotometer (PicoDrop, Cambridge, UK) was used.

The concentration of palladium has been determined using an ICP-MS (model 7700, Agilent Technologies, USA) and the size of PdNCs was obtained by means of an HR-TEM (LIBRA 200 FE, Carl Zeiss).

Electrochemical measurements were carried out using a  $\mu$ -Autolab Type II (EcoChemie BV, Utrecht, Netherlands) controlled by the Autolab GPES software. All measurements were performed at room temperature. Flexible screen-printed carbon electrodes (SPCEs, MicruX Technologies, Spain) with working (7.1 mm<sup>2</sup>) and counter electrodes made of carbon ink and a pseudoreference made of silver were employed. A box connector for thick-film electrodes (MicruX Technologies, Spain) was also employed.

**Synthesis of PdNCs:** The procedure for PdNCs synthesis is as follows (Figure 1A). In a vial protected from light, 0.0125 g of DHLA were added to 10 mL of ultrapure water to which 120  $\mu\text{L}$  of 2 M NaOH had been previously added. It was left stirring at 25 °C for 2 min. Subsequently, 500  $\mu\text{L}$  of a 15 mM  $\text{K}_2\text{PdCl}_4$  solution were added dropwise under stirring, which was maintained for 5 min. Then, 1 mL of 0.5 M  $\text{NaBH}_4$  were added all at once and with vigorous stirring. The molar ratio used was  $\approx 1/8/60$  ( $\text{K}_2\text{PdCl}_4/\text{DHLA}/\text{NaBH}_4$ ).

PdNCs were purified by ultracentrifugation using 10 kDa membrane filters, performing a total of 4 cycles, 15 min each at 5300 rpm, washing with ultrapure water between each cycle. Finally, the PdNCs were stored at room temperature protected from light until further use.

**LAMP Procedure:** The six specific LAMP primers shown in Table S1 (Supporting Information), chosen based in a published work<sup>[63]</sup> were used to amplify the N1 fragment of SARS-CoV-2.<sup>[62]</sup>

The reaction mixture employed was made using WarmStart Colorimetric LAMP 2X Master Mix (DNA & RNA) (New England Biolabs), which contains Bst 2.0 DNA Polymerase, 0.7 mM dUTP, primer mix (1.6  $\mu\text{M}$  each FIP and BIP primer, 0.2  $\mu\text{M}$  each of primers F3 and B3 and 0.4  $\mu\text{M}$  each

of primers Loop F and Loop B), 0.3 U of Uracyl-DNA-Glycosylase (New England Biolabs) and PCR grade dH<sub>2</sub>O (Invitrogen UltraPure™ Distilled Water (DNase/RNase free), Life Technologies). The final volume was 24 μL.

Negative controls were prepared by adding 1 μL of PCR-grade dH<sub>2</sub>O. For positive controls, 1 μL of genomic SARS-CoV-2 RNA (ATCC VR1986D, deposited by the Centers for Disease Control and Prevention, and obtained through BEI Resources, NIAID, NIH: Genomic RNA from SARS-Related Coronavirus 2, Isolate USAWA1/2020, NR52285) solution was added. To bring it to the required concentration, dilutions with PCR-grade dH<sub>2</sub>O were previously made. The amplification reaction was carried out using a thermocycler (Veriti 96 Well Thermal Cycler, Applied Biosystems), starting at 37 °C for 10 min and then increasing the temperature to 65 °C for 30 min. When using UDG, the workflow was modified, adding an initial step of 10 min at 37 °C. Reactions were then kept at 4 °C to improve color contrast.

To avoid possible contamination of the amplifications, all reactions were carried out under sterile conditions using a laminar flow hood. It should be noted that the electrochemical measurements were carried out in a different laboratory and all the instruments used were previously washed with 5% sodium-hypochlorite solution.

For measuring nasopharyngeal exudate samples from human donors, nasopharyngeal swab samples taken at the HUCA were collected on 500 μL TE buffer (10 mM Tris-HCl pH 8.0 and 0.1 mM EDTA). Samples were inactivated at 95 °C for 15 min<sup>[71]</sup> and then kept at −80 °C. This treatment, along with the use of TE buffer, has been proven to be efficient enough for extraction free RNA amplification.<sup>[72]</sup> If needed, samples were diluted with PCR-grade dH<sub>2</sub>O. This study was carried out in accordance with the recommendations of the Ethical Committee on Regional Clinical Research of the Principality of Asturias (Study 2021.526).

**Electrochemical Measurements:** For performing cyclic or linear sweep voltammetry (CV or LSV, respectively), screen-printed electrodes (SPEs) with a SP carbon working electrode were used. A volume of 40 μL of the corresponding solution was deposited on the electrochemical cell covering all the three electrodes (working, auxiliary, and reference). All measurements were carried out at room temperature using a scan rate of 50 mV s<sup>−1</sup>.

**Statistical Analysis:** Results in this study are presented as the mean ± standard deviation except for the value of the size of the nanoclusters, which considers the confidence interval, as stated in Section 2.1. To observe the differences obtained with the RT-LAMP-ED methodology for negative (0 copies μL<sup>−1</sup>) and positive (100 copies μL<sup>−1</sup>) samples, a box and whiskers plot has been performed. The sample size (n) is shown individually for each of the experiments performed. All statistical analyses were performed using Excel 2021 (18.0) software.

## Supporting Information

Supporting Information is available from the Wiley Online Library or from the author.

## Acknowledgements

This work has been supported by the project LIFE of Fondo Supera COVID-19 from Banco de Santander, CRUE and CSIC, as well as by the Spanish Government (MCIN/AEI/10.13039/501100011033) through the I+D+i project PID2020-118376RA-I00, and by the PCTI Program of the Government of the Principality of Asturias and FEDER Program of the European Union (No. AYUD/2021/51289). Also UNIR supported the research, through the collaborative UNIR-UNIOVI project Pneumo.SARS.Detection (2021/2022). E.C.R. thanks for the support of the grant “Beatriz Galindo” (No. BG20/00027) funded by the Ministry of Universities of the Spanish Government. Authors would like to acknowledge the technical support provided by Servicios Científico-Técnicos of the University of Oviedo and by the Service of Microbiology of the Hospital Universitario Central de Asturias. They would also like to thank the Instituto Oftalmológico Fernández-Vega for allowing to use the PICOPET01 spectrophotometer.

## Conflict of Interest

M.T.F.A declares she was one of the founders of Micrux Technologies, a company engaged in the development of miniaturized electrodes and electrochemical/microfluidic equipment and remains a consultant and shareholder. The rest of authors declare no competing financial interest.

## Data Availability Statement

The data that support the findings of this study are available from the corresponding author upon reasonable request.

## Keywords

electrocatalysis, electrochemical detection, isothermal nucleic acid amplification, palladium nanoclusters (PdNCs), RT-LAMP, SARS-CoV-2, screen-printed electrodes

Received: November 16, 2022

Revised: December 21, 2022

Published online: February 17, 2023

- [1] S. Nayak, N. R. Blumenfeld, T. Laksanasopin, S. K. Sia, *Anal. Chem.* **2017**, *89*, 102.
- [2] S. Kumar, M. Nehra, S. Khurana, N. Dilbaghi, V. Kumar, A. Kaushik, K. H. Kim, *Int. J. Nanomed.* **2021**, *16*, 383.
- [3] A. Harmon, C. Chang, N. Salcedo, B. Sena, B. B. Herrera, I. Bosch, L. E. Holberger, *JAMA Network Open* **2021**, *4*, 2126931.
- [4] L. F. O. Team, T. Peto, *EClinicalMedicine* **2021**, *36*, 100924.
- [5] M. M. Serrano, D. N. Rodríguez, N. T. Palop, R. O. Arenas, M. M. Córdoba, M. D. O. Mochón, C. G. Cardona, *J. Clin. Virol.* **2020**, *129*, 104529.
- [6] W. H. Organization, Laboratory testing for coronavirus disease (COVID-19) in suspected human cases: interim guidance, 19 March 2020. <https://apps.who.int/iris/handle/10665/331501> (accessed: October 2022).
- [7] S. Petralia, S. Conoc, *ACS Sens.* **2017**, *2*, 876.
- [8] M. M. Gibani, C. Toumazou, M. Sohbaty, R. Sahoo, M. Karvela, T. K. Hon, S. De Mateo, A. Burdett, F. Leung, J. Barnett, A. Orbeladze, S. Luan, S. Pournias, J. Sun, B. Flower, J. Bedzo-Nutakor, M. Amran, R. Quinlan, K. Skolimowska, C. Herrera, A. Rowan, A. Badhan, R. Klaber, G. Davies, D. Muir, P. Randell, D. Crook, G. P. Taylor, W. Barclay, N. Mughal, et al., *Lancet Microbe* **2020**, *1*, e300.
- [9] R. Augustine, A. Hasan, S. Das, R. Ahmed, Y. Mori, T. Notomi, B. D. Kevadiya, A. S. Thakor, *Biology* **2020**, *9*, 182.
- [10] K. Dhama, K. Karthik, S. Chakraborty, R. Tiwari, S. Kapoor, A. Kumar, P. Thomas, *Pak. J. Biol. Sci.* **2014**, *17*, 166.
- [11] M. N. Esbin, O. N. Whitney, S. Chong, A. Maurer, X. Darzacq, R. Tjian, *RNA* **2020**, *26*, 771.
- [12] Y. P. Wong, S. Othman, Y. L. Lau, S. Radu, H. Y. Chee, *J. Appl. Microbiol.* **2018**, *124*, 626.
- [13] M. Goto, E. Honda, A. Ogura, A. Nomoto, K. I. Hanaki, *BioTechniques* **2009**, *46*, 167.
- [14] N. A. Tanner, Y. Zhang, T. C. Evans, *BioTechniques* **2015**, *58*, 59.
- [15] W. Witkowska McConnell, C. Davis, S. R. Sabir, A. Garrett, A. Bradley-Stewart, P. Jajesniak, G. X. Reboud, Z. Yang, R. Gunson, E. C. Thomson, J. M. Cooper, *Nat. Commun.* **2021**, *12*, 6994.
- [16] J. Reboud, G. Xu, A. Garrett, M. Adriko, Z. Yang, E. M. Tukahebw, C. Rowell, J. M. Cooper, *Proc. Natl. Acad. Sci. USA* **2019**, *116*, 4834.
- [17] Z. Yang, G. Xu, J. Reboud, S. A. Ali, G. Kaur, J. McGiven, N. Boby, P. K. Gupta, P. Chaudhuri, J. M. Cooper, *ACS Sens.* **2018**, *3*, 403.

- [18] K. Hashimoto, M. Inada, K. Ito, *Anal. Biochem.* **2017**, *539*, 113.
- [19] P. Ranjan, A. Singhal, S. Yadav, N. Kumar, S. Murali, S. K. Sanghi, R. Khan, *Int. Rev. Immunol.* **2021**, *40(1-2)*, 126.
- [20] E. T. Da Silva, D. E. Souto, J. T. Barragan, J. de F. Giarola, A. C. de Moraes, L. T. Kubota, *ChemElectroChem* **2017**, *4*, 778.
- [21] R. G. Ramírez-Chavarría, E. Castillo-Villanueva, B. E. Alvarez-Serna, J. Carrillo-Reyes, R. M. Ramírez-Zamora, G. Buitrón, L. Alvarez-Icaza, *J. Environ. Chem. Eng.* **2022**, *10*, 107488.
- [22] H. Kong, W. Zhang, J. Yao, C. Li, R. Lu, Z. Guo, J. Li, C. Y. Li, C. Zhang, L. Zhou, *Sens. Actuators, B* **2021**, *329*, 129118.
- [23] V. T. Thu, B. Q. Tien, D. T. N. Nga, L. C. Thanh, T. C. Le, T. L. Dai, *RSC Adv.* **2018**, *8*, 25361.
- [24] J. Zheng, P. R. Nicovich, R. M. Dickson, *Annu. Rev. Phys. Chem.* **2007**, *58*, 409.
- [25] Z. Luo, K. Zheng, J. Xie, *Chem. Commun.* **2014**, *50*, 5143.
- [26] X. L. Guevel, O. Tagit, C. E. Rodríguez, V. Trouillet, M. P. Leal, N. Hildebrandt, *Nanoscale* **2014**, *6*, 8091.
- [27] K. Kwak, S. S. Kumar, K. Pyo, D. Lee, *ACS Nano* **2014**, *8*, 671.
- [28] T. K. Moon, S. Y. Jeong, Y. C. Kang, J. H. Lee, *ACS Appl. Mater. Interfaces* **2019**, *11*, 32169.
- [29] H. Tsunoyama, Y. Yamano, C. Zhang, M. Komori, T. Eguchi, A. Nakajima, *Top. Catal.* **2018**, *61(1-2)*, 126.
- [30] Y. Peng, P. Wang, L. Luo, L. Liu, F. Wang, *Materials* **2018**, *11*, 191.
- [31] A. Lores-Padín, B. Fernández, L. Álvarez, H. González-Iglesias, I. Lengyel, R. Pereiro, *Talanta* **2021**, *221*, 121489.
- [32] J. Yu, S. Choi, C. I. Richards, Y. Antoku, R. M. Dickson, *Photochem. Photobiol.* **2008**, *84*, 1435.
- [33] K. Zheng, J. Xie, *Trends Chem.* **2020**, *2*, 665.
- [34] J. Durand, E. Teuma, M. Gómez, *Eur. J. Inorg. Chem.* **2008**, *23*, 3577.
- [35] J. Athilakshmi, S. Ramanathan, D. K. Chand, *Tetrahedron Lett.* **2008**, *49*, 5286.
- [36] X. Gao, G. Yu, L. Zheng, C. Zhang, H. Li, T. Wang, P. An, M. Liu, X. Qiu, W. Chen, *ACS Appl. Energy Mater.* **2019**, *2*, 966.
- [37] J. Cai, R. Javed, D. Ye, H. Zhao, J. Zhang, *J. Mater. Chem. A* **2020**, *8*, 22467.
- [38] F. He, Y. Liu, Q. Cai, J. Zhao, *New J. Chem.* **2020**, *44*, 16135.
- [39] S. Zhao, H. Zhang, S. D. House, R. Jin, J. C. Yang, R. Jin, *ChemElectroChem* **2016**, *3*, 1225.
- [40] T. Wang, A. Chutia, D. J. Brett, P. R. Shearing, G. He, G. Chai, I. P. Parkin, *Energy Environ. Sci.* **2021**, *14*, 2639.
- [41] Z. Tang, W. Wu, K. Wang, *Catalysts* **2018**, *8*, 65.
- [42] A. U. Nilekar, M. Mavrikakis, *Surf. Sci.* **2008**, *602*, L89.
- [43] J. Zhang, M. B. Vukmirovic, Y. Xu, M. Mavrikakis, R. R. Adzic, *Angew. Chem.* **2005**, *117*, 2170.
- [44] J. K. Nørskov, J. Rossmeisl, A. Logadottir, L. Lindqvist, J. R. Kitchin, T. Bligaard, H. Jónsson, *J. Phys. Chem. B* **2004**, *108*, 17886.
- [45] M. Harada, H. Noguchi, N. Zanetakis, S. Takakusagi, W. Song, K. Uosaki, *Sci. Technol. Adv. Mater.* **2011**, *12*, 044606.
- [46] M. C. Aguirre, B. L. Rivas, L. M. Fabietti, S. E. Urreta, *J. Appl. Electrochem.* **2019**, *49*, 1.
- [47] G. Yang, D. Chen, P. Lv, X. Kong, Y. Sun, Z. Wang, Z. Yuan, H. Liu, J. Yang, *Sci. Rep.* **2016**, *6*, 35252.
- [48] N. F. Atta, M. F. El-Kady, A. Galal, *Sens. Actuators, B* **2009**, *141*, 566.
- [49] A. A. Abdelwahab, M. Abdel-Hakim, M. Abdelmottaleb, A. S. Elshahawy, *Electroanalysis* **2019**, *31*, 1672.
- [50] L. Ma, L. Zhou, Y. He, L. Wang, Z. Huang, Y. Jiang, J. Gao, *Electroanalysis* **2018**, *30*, 1801.
- [51] C. Toyos-Rodríguez, A. Adawy, F. J. Alonso, A. de la Escosura-Muñiz, *Biosens. Bioelectron.* **2022**, *200*, 113926.
- [52] N. Yang, P. Liu, C. Cai, R. Zhang, K. Sang, P. Shen, Y. Huang, Y. Lu, *Enzyme Microb. Technol.* **2021**, *149*, 109855.
- [53] A. P. M. Ferreira, A. P. M., L. N. dos Santos Pereira, I. S. da Silva, S. M. Tanaka, A. A. Tanaka, L. Angnes, *Electroanalysis* **2014**, *26*, 2138.
- [54] D. D. Qin, Y. Tang, G. Ma, L. Qin, C. L. Tao, X. Zhang, Z. Tang, *Int. J. Hydrogen Energy* **2021**, *46*, 25771.
- [55] A. Mahata, K. S. Rawat, I. Choudhuri, B. Pathak, *Catal. Sci. Technol.* **2016**, *6*, 7913.
- [56] H. P. Choo, K. Y. Liew, H. Liu, *J. Mater. Chem.* **2002**, *12*, 934.
- [57] X. Meng, Z. Liu, M. Zhu, R. Jin, *Nanoscale Res. Lett.* **2012**, *7*, 277.
- [58] D. B. Sepa, M. V. Vojnovic, L. M. Vracar, A. Damjanovic, *Electrochim. Acta* **1987**, *32*, 129.
- [59] J. Cui, F. Li, Z. L. Shi, *Nat. Rev. Microbiol.* **2019**, *17*, 181.
- [60] W. E. Huang, B. Lim, C. C. Hsu, D. Xiong, W. Wu, Y. Yu, H. Jia, Y. Wang, Y. Zeng, M. Ji, H. Chang, X. Zhang, H. Wang, Z. Cui, *Microb. Biotechnol.* **2020**, *13*, 950.
- [61] A. González-López, M. D. Cima-Cabal, P. Rioboó-Legaspi, E. Costa-Rama, M. M. García-Suárez, M. T. Fernández-Abedul, *Anal. Chem.* **2022**, *94*, 13061.
- [62] V. L. T. Dao, K. Herbst, K. Boerner, M. Meurer, L. P. Kremer, D. Kirmaier, A. Freistaedter, D. Papagiannidis, C. Galmozzi, M. Stanifer, S. Boulant, S. Klein, P. Chlanda, D. Khalid, I. B. Miranda, P. Schnitzler, H. G. Kräusslich, M. Knop, S. A. Anders, *Sci. Transl. Med.* **2020**, *12*, 7075.
- [63] Y. Wang, D. Liu, J. Deng, Y. Wang, J. Xu, C. Ye, *Anal. Chim. Acta* **2017**, *996*, 74.
- [64] X. Gao, B. Sun, Y. Guan, *Anal. Bioanal. Chem.* **2019**, *411*, 1211.
- [65] New England Biolabs, <https://international.neb.com/faqs/2021/07/27/amplification-occurred-in-my-ntc-samples-following-isothermal-incubation-what-happened> (accessed: November 2022).
- [66] C. Zhang, T. Zheng, H. Wang, W. Chen, X. Huang, J. Liang, L. Qiu, D. Han, W. Tan, *Anal. Chem.* **2021**, *93*, 3325.
- [67] X. Zhu, X. Wang, L. Han, T. Chen, L. Wang, H. Li, S. Li, L. He, X. Fu, S. Chen, M. Xing, H. Chen, Y. Wang, *Biosens. Bioelectron.* **2020**, *166*, 112437.
- [68] A. E. Urusov, A. V. Zherdev, B. B. Dzantiev, *Biosensors* **2019**, *9*, 89.
- [69] New England Biolabs, <https://international.neb.com/faqs/2021/07/27/what-are-the-advantages-of-using-standard-lamp-neb-e1700-m1708-e1708-over-ph-based-colorimetric-lamp-neb-m1800-m1804> (accessed: November 2022).
- [70] B. Gates, TED Conferences, **2022**. [https://www.ted.com/talks/bill\\_gates\\_we\\_can\\_make\\_covid\\_19\\_the\\_last\\_pandemic](https://www.ted.com/talks/bill_gates_we_can_make_covid_19_the_last_pandemic) (accessed: 16 November 2022).
- [71] C. P. Rubio, L. Franco-Martínez, C. S. Resalt, A. Torres-Cantero, I. Martínez-Morata, E. Bernal, M. J. Alcaraz, M. R. Vicente-Romero, S. Martínez-Subiela, A. Tvari-jonavicute, J. J. Cerón, *Int. J. Infect. Dis.* **2021**, *108*, 413.
- [72] D. R. E. Ranoa, R. L. Holland, F. G. Alnaji, K. J. Green, L. Wang, C. B. Brooke, M. D. Burke, T. M. Fan, P. J. Hergenrother, *bioRxiv* **2020**.